


LETTER

Open Access



Electrochemical activity of glassy carbon electrode modified with ZnO nanoparticles prepared Via *Senna Alata L.* leaf extract towards antiretroviral drug

Harits Atika Ariyanta^{1*} , Fakhrrur Roji¹ and Dewangga Oky Bagus Apriandanu²

Abstract

The phytosynthesis method was used to prepare ZnO nanoparticles (ZnO NPs) via *Senna alata L.* leaf extract (SALE) by involving alkaloids, which play an essential role as a source of weak bases during the formation reaction of NPs. ZnO NPs on glassy carbon electrodes (GCE/ZnO NP) have been introduced to investigate its electrochemical activity towards the antiretroviral drug, lamivudine (3TC). Several characterization techniques, such as Fourier Transform Infra-Red (FTIR), X-Ray Diffraction (XRD), Scanning Electron Microscopy (SEM), Energy Dispersive X-Ray Spectroscopy (EDS), and Dynamic Light Scattering (DLS) techniques were employed to analyze the properties of GCE/ZnO NPs. As a result, ZnO NPs in spherical shape showed a high purity crystalline hexagonal wurtzite structure with a particle diameter of 40–60 nm. A Cyclic Voltammetry (CV) measurement confirmed that the electrochemical reduction of 3TC on GCE/ZnO NPs exhibited an excellent linear range of 10–300 μM with a detection limit of 1.902 μM , quantitation limit of 6.330 μM , and sensitivity of 0.0278 $\mu\text{A}/\mu\text{M}$. Thus, this research suggests a facile method for the preparation of material-based ZnO NPs as a promising antiretroviral drug sensors due to their excellent electrochemical properties.

Keywords: ZnO nanoparticles, Lamivudine, Electrochemical sensor, Phytosynthesis, Green synthesis

Introduction

Lamivudine (2'-deoxy-3'-thiacytidine, 3TC) is a nucleoside analog reverse transcriptase inhibitor (NRTI) drug that is actively against retroviruses, including human immunodeficiency virus type 1 (HIV-1), human immunodeficiency virus type 2 (HIV-2), and hepatitis B virus (HBV) [1]. 3TC inhibits the virus growth through the DNA chain-breaking by forming intracellular triphosphate to prevent the multiplication of viral DNA in the host [2–4]. However, the use of 3TC in long-term use leads to the emergence of mutant HBV resistance. Drug-resistant genotypes with mutations at codons rt80, rt173,

rt180, and rt204 are rapidly selected by 3TC monotherapy of HBV, occurring in 15% of treated people after one year and up to 80% after 3 years. In addition, selection of mutants not identified by hepatitis B surface antigen (HBsAg) testing may obscure the detection of HBV infection after 3TC treatment. Individuals with these mutations may spread HBV that is resistant to the immunological responses generated by the HBV vaccine [5].

Based on their medicinal and pharmacological significance, evaluating appropriate levels of 3TC in biological fluids and pharmaceutical preparations is tremendously essential. The analytical methods for assessing 3TC levels have been repeatedly reported, such as spectrophotometry [6, 7], chromatography [8], electrochemistry [9–12], etc. The chromatography and spectrophotometry methods have presented good selectivity and detection limits. However, several flaws, such as time-consuming,

*Correspondence: harits@staff.gunadarma.ac.id

¹ Department of Pharmacy, Universitas Gunadarma, Depok 16424, Indonesia
Full list of author information is available at the end of the article

relatively expensive, requiring a complicated analysis step have been investigated. Therefore, well-qualified personnel are required to develop other analytical methods such as electrochemistry due to its low cost, easy to handle, and better reproducibility [13, 14]. Additionally, in the electrochemical method, modification of the electrode surface using electroconductive materials should be taken into account to optimize electron transfer between the analyte and the sensing surface. Also, electroconductive materials have enhanced the surface area of the electrode to produce superior sensitivity [15, 16].

ZnO NPs are materials with good electrical conductivity, negligible toxicity, high electron transfer kinetics, and excellent electrocatalytic activity against biomolecules [17]. Currently, phytosynthesis has been considered as one of the prospective methods to prepare ZnO NPs compared to the conventional one due to its harmless route [18] since it uses no toxic chemicals [19] such as sodium dodecyl sulfate (SDS), tetramethylammonium bromide (CTAB) [20, 21], and polyvinylpyrrolidone (PVP) [22]. Additionally, this method utilizes the secondary metabolite content of plant extracts as a source of weak bases, chelating agents, stabilizing agents, and reducing agents [23, 24].

In this work, ZnO NPs were synthesized using leaf extract of *Senna Alata L.* (SALE), an angiosperm belonging to the family of Fabaceae [25], which contains secondary metabolites in the form of alkaloids, flavonoids, and saponins that act as sources of weak bases, chelating agents, and stabilizing agents during the reaction. Furthermore, ZnO NPs were used to modify the surface of the glassy carbon electrode (GCE). The electrochemical activity of GCE/ZnO NPs was analyzed against 3TC. The sensitivity and detection limit were also investigated by electrochemical measurements.

Experimental section

Materials

Senna Alata L. leaves were obtained from Cirebon district, West Java, Indonesia, and further determined at the Research Center for Biology, LIPI, Indonesia. Zinc nitrate hexahydrate ($\text{Zn}(\text{NO}_3)_2 \cdot 6\text{H}_2\text{O}$), potassium hydrogen phosphate (K_2HPO_4), potassium dihydrogen phosphate (KH_2PO_4), methanol, and n-hexane were purchased from Merck. Lamivudine was obtained from the Indonesian Pharmacopoeia Comparative Standard (BPFI). The double distilled water used in this research was purified with Millipore Direct-Q® 5 UV. All chemicals were used as received without purification.

Preparation of SALE

Senna Alata L. leaf was washed, dried, and mashed to obtain powder. 50 g of powders were macerated in

250 mL of methanol for 7 days by continuously stirring. Afterward, the filtrate was filtered using Whatman no. 40 filters and fractionated in n-hexane with a volume ratio of 1:1. The result was evaporated using a vacuum rotary evaporator and dissolved into 100 mL of distilled water. Finally, the obtained SALE was stored at 4 °C for the preparation of ZnO NPs by the phytosynthesis method.

Phytosynthesis of ZnO NPs

ZnO NPs were fabricated via phytosynthesis method through a sol-gel process. SALE was added to $\text{Zn}(\text{NO}_3)_2$ 0.015 M to obtain 100 mL of the mixture with a volume ratio of 1:9 (v/v). The SALE sol was formed by heating at 60 °C for 2 h. The sol was further heated at 120 °C for 6 h and centrifuged to form a gel. Finally, the gel was calcined at 500 °C for 4 h to obtain white powders of ZnO NPs.

Fabrication of the GCE/ZnO NPs

The GCE surface was manually polished with alumina slurry for a minute and washed with ultrapure water. Then, the GCE was sonicated in methanol for 10 min, then rinsed with ultrapure water. ZnO NPs were dispersed in ethanol (4 mg/mL). Afterward, it was deposited on the surface of GCE (2 mm diameter) by the drop-casting technique. Finally, GCE/ZnO NPs were dried at 60 °C.

Electrochemical measurement

The three-electrode system was used for the electrochemical study of prepared electrodes towards 3TC. The GCE/ZnO NPs, platinum wire, and Ag/AgCl served as the working, counter, and reference electrodes, respectively. The electrolyte was a 0.1 M phosphate buffer solution (PBS) at pH ranging from 5 to 9 prepared by mixing quantitative amounts of KH_2PO_4 and K_2HPO_4 in ultrapure water. The electrochemical measurements were performed using CV techniques at a range potential of – 1.2 to 0.5 V.

Characterization

An Autolab PGSTAT204 was used to perform a three-electrode system for voltammetric measurements. The morphologies of the sample were characterized by Scanning Electron Microscopy-Energy Dispersive X-ray Spectrometer (SEM-EDS, JEOL JSM 6510 LA). In contrast, the sample structure was analyzed using Powder X-Ray Diffraction (XRD, Miniflex 600-Rigaku X-Ray Analytical Instrument) and Fourier Transform Infra-Red spectroscopy (FTIR, IR Prestige-21 Shimadzu). Malvern Zetasizer Nano ZSP, a particle size analyzer, determined the particle size distribution.

Results and discussion

Characterization of SALE and ZnO NPs

Figure 1a shows that the FTIR spectrum of ZnO NPs exhibit absorption peaks at wavenumbers of 3442, 2911, 1625, 1054, and 489 cm^{-1} , which correspond to the vibration of O–H stretching, C–H (sp^3) stretching, N–H bending, C–N stretching, and Zn–O stretching, respectively [26, 27]. The O–H stretching vibration is assigned to the residual secondary metabolites of SALE in the form of flavonoids, saponins, and polyphenols and the adsorption of H_2O from the atmosphere [1, 23]. The N–H bending and C–N stretching vibrations indicate the presence of alkaloids that play an essential role as a source of weak bases in the phytosynthesis of ZnO NPs [23, 28]. Also, Zn–O stretching vibrations indicate that ZnO NPs have been successfully formed [29–32] through the phytosynthesis method using SALE.

Moreover, the XRD diffraction pattern in Fig. 1b clearly shows that all the diffraction peaks at (100), (002), (101), (102), (110), (103), (200), (112), and (201) planes were indexed to the crystalline ZnO hexagonal wurtzite structure (JCPDS Card No. 36–1451). The average crystallite size of ZnO NPs was calculated from the following Scherrer's formula [33]:

$$D = \frac{0.9\lambda}{\beta \cos \theta}$$

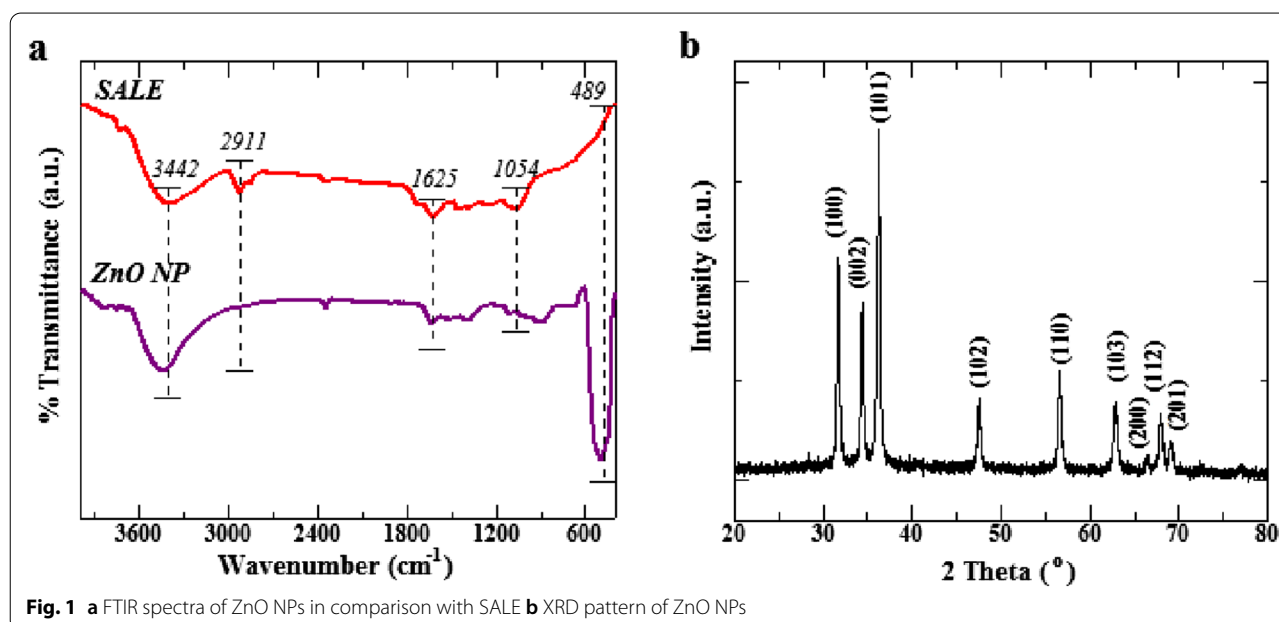
where, D is the crystallite size average, λ is the wavelength of the X-rays (0.15406 nm), β is the FWHM and θ is the diffraction angle. The average value of the crystallite size of ZnO NPs was found to be 18.87 nm.

The SEM images in Fig. 2a depict the ZnO NPs prepared from SALE in a spherical shape with a particle size range of 40–60 nm. The presence of zinc and oxygen by elemental mapping was studied using EDS with an atomic composition ratio of 53.6: 46.4. No other elements from the impurities were observed, which indicates the formation of ZnO NPs with high purity in a homogeneous spherical shape (Fig. 2a,b). In addition, the particle distribution curve obtained by the dynamic light scattering technique shows that the hydrodynamic size of the ZnO NPs was determined to be 68.061 nm (Fig. 2c).

The electrochemical activity of GCE/ZnO NPs towards 3TC

The electrochemical activity of GCE/ZnO NPs against 3TC in 0.1 M PBS (pH 7) was determined through cyclic voltammetry (CV). Figure 3 demonstrates that GCE and GCE/ZnO NPs both had a reduction peak current of 3TC at a reduction peak potential of -0.906 and -1.095 V, respectively, under the same experimental conditions. The improved conductivity and electrochemical characteristics of ZnO NPs resulted in greater electron transport, leading to a higher current response of GCE/ZnO NPs when compared to GCE.

The CV response of 3TC in 0.1 M PBS at the surface of the prepared electrode with different pH from 5 to 9 was performed in Fig. 4a. The highest current response was obtained at an optimal pH level of 7 through a reduction peak of -1.095 V (Fig. 4b). In addition, Fig. 4c shows that the more alkaline in the pH system, the peak of the cathodic current shifts to a more negative potential, indicating the involvement of protons in the redox reaction



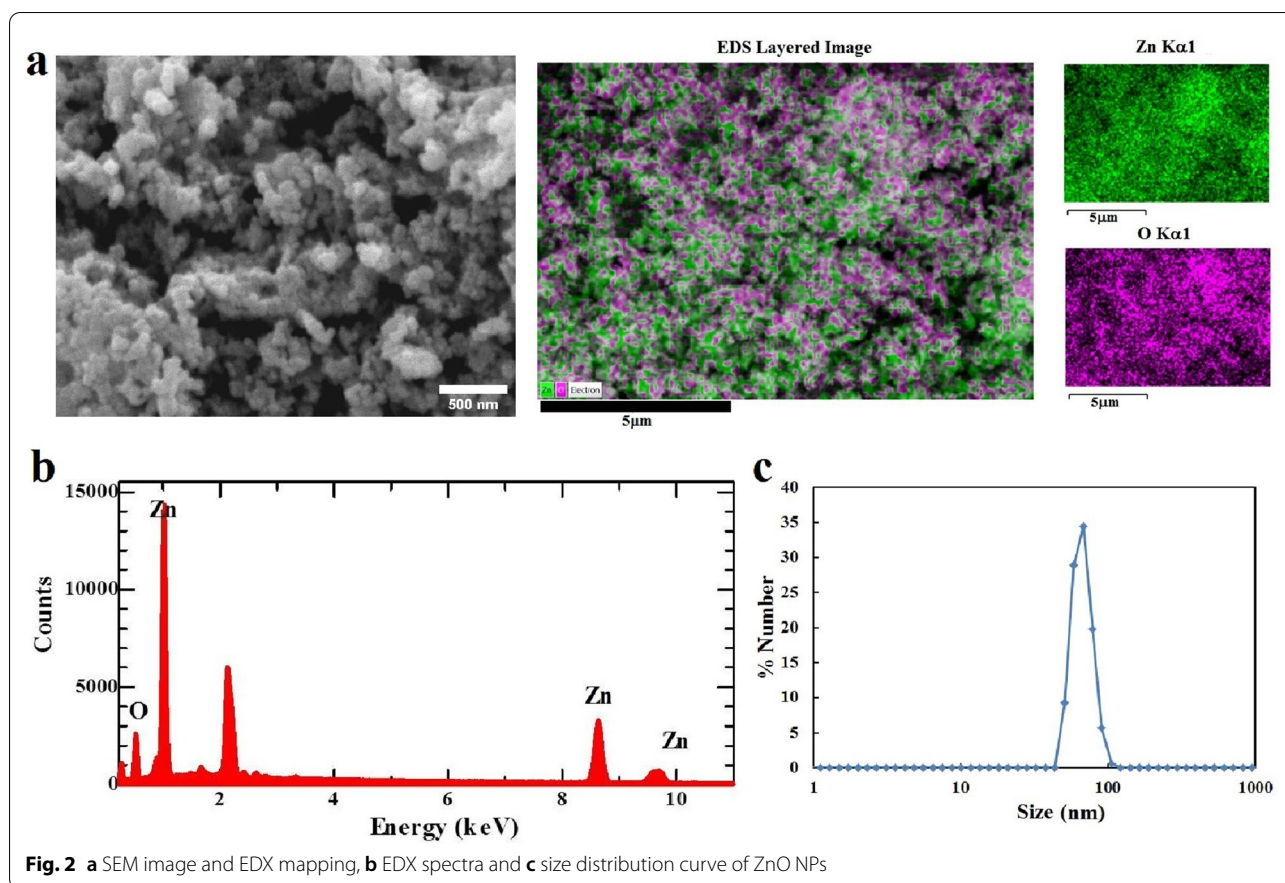


Fig. 2 a SEM image and EDX mapping, b EDX spectra and c size distribution curve of ZnO NPs

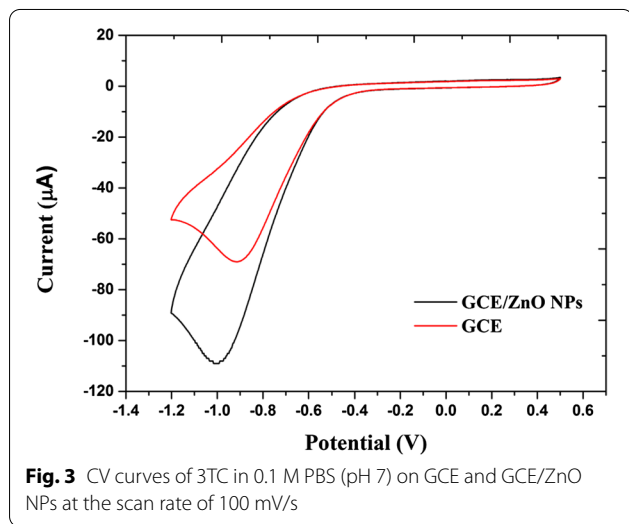


Fig. 3 CV curves of 3TC in 0.1 M PBS (pH 7) on GCE and GCE/ZnO NPs at the scan rate of 100 mV/s

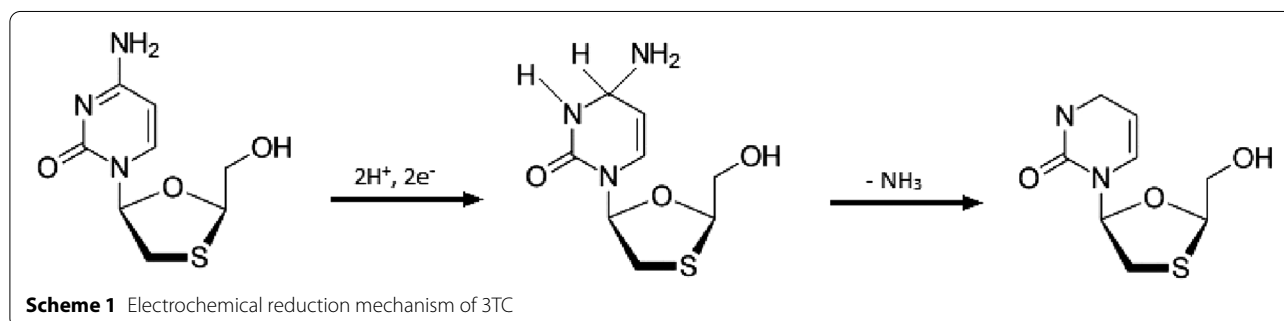
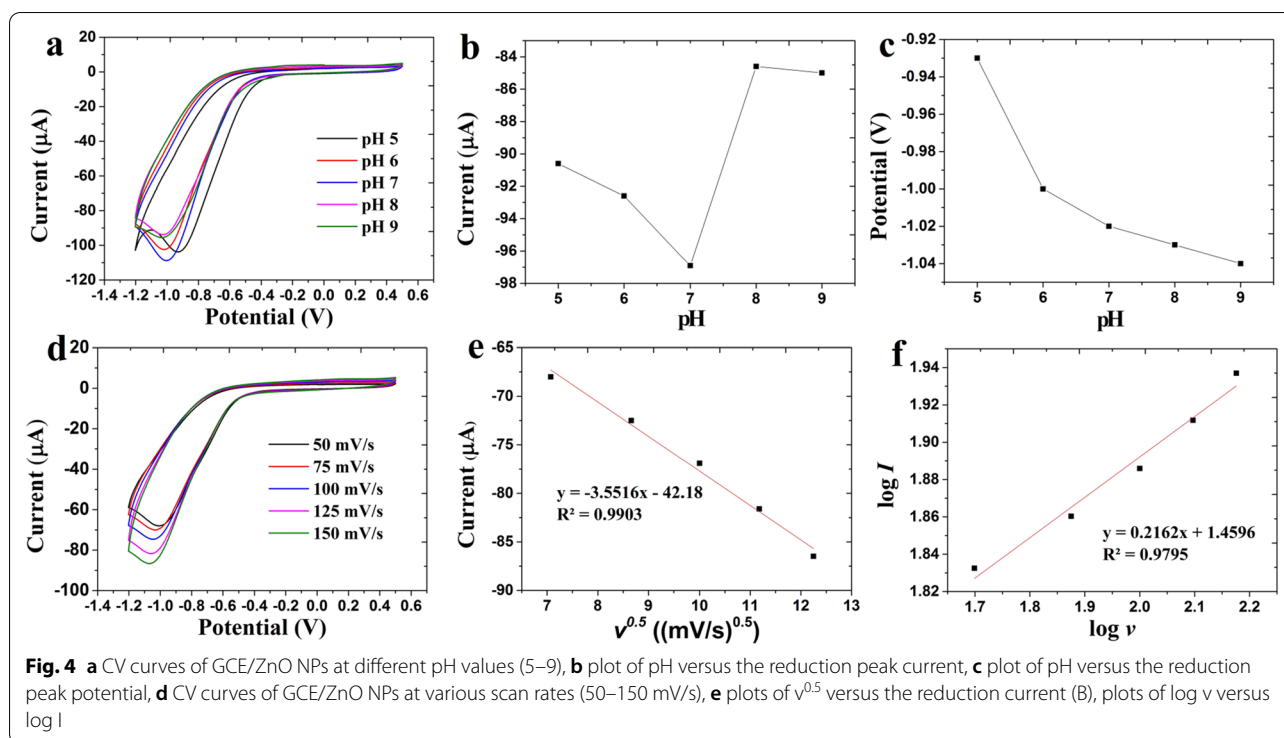
[34]. According to the reaction mechanism (Scheme 1), the reduction peak results from the reduction of 3TC in GCE/ZnO NPs, involving two electron transfers. The C=N bond from 3TC is reduced, followed by the deamination process. [35].

The kinetics of electron transfer at the electrode surface was determined using the Randles–Sevcik Eq. (1) in the scan rate range of 50–150 mV/s [36]:

$$I_p = 0.4463 n F A c \left(\frac{n F \nu D}{RT} \right)^{0.5} \quad (1)$$

where I_p is the peak current (A), n is the number of electrons transferred peroxidation or reduction of one analyte molecule; A is the electrode surface area (cm^2), D is the analyte diffusion coefficient (cm^2/s), ν is the scan rate (V/s), c is the concentration of analyte in bulk solution (mol/cm^3), R is the ideal gas constant, and T is the temperature (K).

The reduction peak current of 3TC was increased linearly with different scan rates (Fig. 4d). The plot between anodic and cathodic peak currents versus the root of the scan rate in the Randles–Sevcik equation shows a linear relationship, indicating the kinetics of electron transfer controlled by the diffusion process [37]. Figure 4e presents a linear plot between the reduction peak current of 3TC and the root of the scan rate with a correlation coefficient of 0.9903. This result indicates that the electron transfer process at the electrode



is diffusion controlled. The plot between the logarithm of the scan rate versus the logarithm of the peak current in the Randles–Sevcik equation was also investigated to understand the possibility of an adsorption process on the electrode surface. If the gradient value in the resulting linear equation is close to 0.5, then the redox reaction is completely diffusion controlled. However, if the gradient value is more than 0.5, it indicates an adsorption process [38]. Figure 4f shows the linear equation between $\log v$ and $\log I$ at a gradient value of 0.2162. This result suggests that the 3TC reduction process on the surface of GCE/ZnO NPs is not controlled by adsorption.

For the calibration curve, CV measurement was carried out in the 3TC concentration range of 10–300 μM ,

as seen in Fig. 5a. The calibration curve equation was obtained to be $y = -0.0278x - 81$ ($R^2 = 0.9987$), indicating excellent linearity of GCE/ZnO NPs towards 3TC in the low concentration range (10–75 μM) to high (300 μM) with a remarkable detection limit of 1.902 μM , a quantitation limit of 6.330 μM , and a sensitivity of 0.0278 $\mu\text{A}/\mu\text{M}$. The detection limit was obtained from three times the standard deviation divided by the slope of the calibration curve, whereas the limit quantitation was obtained using the ten times. Also, the sensitivity is determined from the slope on the calibration curve [39].

The repeatability of GCE/ZnO NPs was investigated at 40 μM 3TC using the same fabricated electrode (Fig. 5b). The calculated relative standard deviation

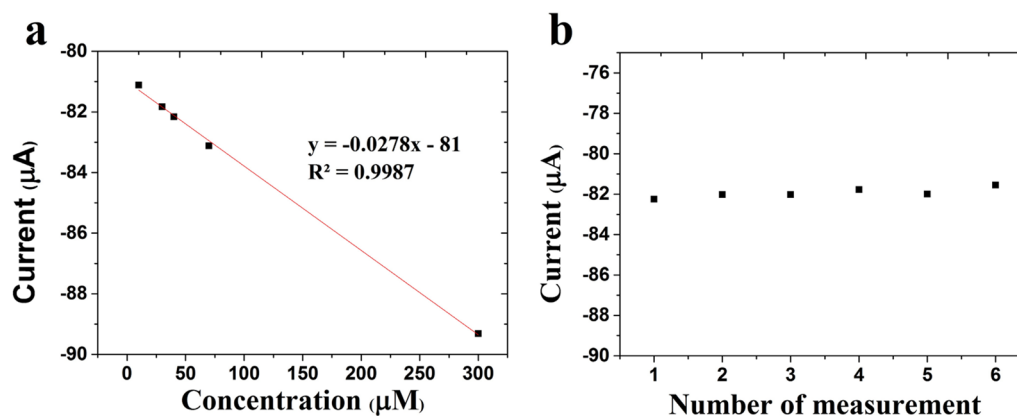


Fig. 5 **a** Calibration curve of the 3TC concentration versus the reduction peak current and **b** repeatability studies of GCE/ZnO NPs for 3TC in 0.1 M PBS (pH 7)

(RSD) was found to be 1.26% ($n=6$). This result shows the good repeatability with GCE/ZnO NPs for 3TC in 0.1 M PBS (pH 7).

Conclusions

In this work, ZnO NPs have been successfully synthesized by phytosynthesis method using SALE by involving alkaloids which play an important role as a source of weak bases. GCE modified with ZnO NPs showed excellent electrochemical activity toward 3TC at a good linear range of 10–300 μM with a detection limit of 1.902 μM , quantitation limit of 6.330 μM , and sensitivity of 0.0278 $\mu\text{A}/\mu\text{M}$. The excellent electrochemical activity of the prepared electrode might be attributed to the good electrical conductivity and high electron transfer kinetics of ZnO NPs. Thus, this research suggests a facile method for the preparation of material-based ZnO NPs as promising antiretroviral drug sensors due to their excellent electrochemical properties.

Acknowledgements

Not applicable.

Author contributions

HAA: conceptualization; funding acquisition; methodology; roles/writing—original draft; FR: data curation; formal analysis; investigation; DOBA: writing—review and editing; resources. All the authors have read and approved the final manuscript.

Funding

This work was funded by Rektor Universitas Gunadarma No. 22/SK/REK/UG/2021.

Availability of data and materials

The datasets used and/or analysed during the current study are available from the corresponding author on reasonable request.

Declarations

Competing interests

The authors declare that they have no competing interests.

Author details

¹Department of Pharmacy, Universitas Gunadarma, Depok 16424, Indonesia.

²Department of Chemistry, Faculty of Mathematics and Natural Sciences, Universitas Indonesia, Depok 16424, Indonesia.

Received: 2 April 2022 Accepted: 3 May 2022

Published online: 17 May 2022

References

- Ariyanta HA, Chodijah S, Roji F, Kurnia A, Apriandanu DOB (2022) The role of *Andrographis paniculata* L. modified nanochitosan for lamivudine encapsulation efficiency enhancement and in vitro drug release study. *J Drug Deliv Sci Technol* 67:103016. <https://doi.org/10.1016/j.jddst.2021.103016>
- Ngilirabanga JB, Aucamp M, Samsodien H (2021) Mechanochemical synthesis and characterization of Zidovudine-lamivudine solid dispersion (binary eutectic mixture). *J Drug Deliv Sci Technol* 64:102639. <https://doi.org/10.1016/j.jddst.2021.102639>
- Sneha R, Vedha Hari BN, Ramya Devi D (2018) Design of antiretroviral drug-polymeric nanoparticles laden buccal films for chronic HIV therapy in paediatrics. *Colloids Interface Sci Commun* 27:49–59. <https://doi.org/10.1016/j.colcom.2018.10.004>
- Shahabadi N, Khorshidi A, Zhaleh H, Kashanian S (2018) Synthesis, characterization, cytotoxicity and DNA binding studies of Fe₃O₄@SiO₂ nanoparticles coated by an antiviral drug lamivudine. *J Drug Deliv Sci Technol* 46:55–65. <https://doi.org/10.1016/j.jddst.2018.04.016>
- Beck IA, Payant R, Ngo-giang-huong N, Khamduang W, Laomanit L, Jourdain G, Frenkel LM (2016) Development and validation of an oligonucleotide ligation assay to detect lamivudine resistance in hepatitis B virus. *J Virol Methods* 233:51–55. <https://doi.org/10.1016/j.jviromet.2016.03.014>
- Kepekci Tekkeli SE (2013) Extractive spectrophotometric method for the determination of lamivudine and zidovudine in pharmaceutical preparations using bromocresol purple. *J Chem* 2013:1–6. <https://doi.org/10.1155/2013/484389>
- Serag A, Hasan MA, Tolba EH, Abdelzaher AM, Abo Elmaaty A (2021) Analysis of the ternary antiretroviral therapy dolutegravir, lamivudine and abacavir using UV spectrophotometry and chemometric tools. *Spectrochim Acta Part A Mol Biomol Spectrosc* 264:120334. <https://doi.org/10.1016/j.saa.2021.120334>

8. Bahrami G, Mirzaeei S, Kiani A, Mohammadi B (2005) High-performance liquid chromatographic determination of lamivudine in human serum using liquid-liquid extraction; application to pharmacokinetic studies. *J Chromatogr B Anal Technol Biomed Life Sci* 823:213–217. <https://doi.org/10.1016/j.jchromb.2005.06.044>
9. Prasad BB, Singh K (2017) Molecularly imprinted polymer-based core-shells (solid vs hollow) @ pencil graphite electrode for electrochemical sensing of certain anti-HIV drugs. *Sensors Actuators B Chem* 244:167–174. <https://doi.org/10.1016/j.snb.2016.12.109>
10. Leandro KC, Moreira JC, Farias PAM (2013) Differential pulse voltammetric studies on lamivudine: an antiretroviral drug. *Am J Anal Chem* 04:47–51. <https://doi.org/10.4236/ajac.2013.46a007>
11. Chihava R, Apath D, Moyo M, Shumba M, Chitsa V, Tshuma P (2020) One-Pot Synthesized nickel-cobalt sulfide-decorated graphene quantum dot composite for simultaneous electrochemical determination of antiretroviral drugs: lamivudine and tenofovir disoproxil fumarate. *J Sensors*. <https://doi.org/10.1155/2020/3124102>
12. Wang Y, Zhou C, Chen J, Fu Z, Niu J (2019) Bicarbonate enhancing electrochemical degradation of antiviral drug lamivudine in aqueous solution. *J Electroanal Chem* 848:113314. <https://doi.org/10.1016/j.jelechem.2019.113314>
13. Jesu Amalraj AJ, Narasimha Murthy U, Sea-Fue W (2021) Ultrasensitive electrochemical detection of an antibiotic drug furaltadone in fish tissue with a ZnO-ZnCo₂O₄ self-assembled nano-heterostructure as an electrode material. *Microchem J* 169:106566. <https://doi.org/10.1016/j.microc.2021.106566>
14. Ariyanta HA, Ivandini TA, Yulizar Y (2021) Poly(methyl orange)-modified NiO/MoS₂/SPCE for a non-enzymatic detection of cholesterol. *FlatChem* 29:100285. <https://doi.org/10.1016/j.flatc.2021.100285>
15. Ansari AA, Malhotra BD (2022) Current progress in organic-inorganic hetero-nano-interfaces based electrochemical biosensors for healthcare monitoring. *Coord Chem Rev* 452:214282. <https://doi.org/10.1016/j.ccr.2021.214282>
16. Aghari S, Kumar Gautam R, Kumar Singh A, Tiwari I (2022) Nanoscale materials-based hybrid frameworks modified electrochemical biosensors for early cancer diagnostics: an overview of current trends and challenges. *Microchem J* 172:106980. <https://doi.org/10.1016/j.microc.2021.106980>
17. Shetti NP, Bukkitgar SD, Reddy KR, Reddy CV, Aminabhavi TM (2019) ZnO-based nanostructured electrodes for electrochemical sensors and biosensors in biomedical applications. *Biosens Bioelectron* 141:111417. <https://doi.org/10.1016/j.bios.2019.111417>
18. Chan YY, Pang YL, Lim S, Chong WC (2021) Facile green synthesis of ZnO nanoparticles using natural-based materials: properties, mechanism, surface modification and application. *J Environ Chem Eng* 9:105417. <https://doi.org/10.1016/j.jece.2021.105417>
19. Sharma D, Sabala MI, Kanchi S, Bissety K, Skelton AA, Honarparvar B (2018) Green synthesis, characterization and electrochemical sensing of silymarin by ZnO nanoparticles: experimental and DFT studies. *J Electroanal Chem* 808:160–172. <https://doi.org/10.1016/j.jelechem.2017.11.039>
20. Pichon BP, Leuvre C, Ihiwakrim D, Tichit D, Gérardin C (2011) Films of tunable ZnO nanostructures prepared by a surfactant-mediated soft synthesis route. *J Phys Chem C* 115:23695–23703. <https://doi.org/10.1021/jp2072149>
21. Thilagavathi T, Geetha D (2014) Nano ZnO structures synthesized in presence of anionic and cationic surfactant under hydrothermal process. *Appl Nanosci* 4:127–132. <https://doi.org/10.1007/s13204-012-0183-8>
22. Tang H, Yan M, Ma X, Zhang H, Wang M, Yang D (2006) Gas sensing behavior of polyvinylpyrrolidone-modified ZnO nanoparticles for trimethylamine. *Sensors Actuators B Chem* 113:324–328. <https://doi.org/10.1016/j.snb.2005.03.024>
23. Ariyanta HA, Ivandini TA, Yulizar Y (2021) Novel NiO nanoparticles via phytosynthesis method: structural, morphological and optical properties. *J Mol Struct* 1227:129543. <https://doi.org/10.1016/j.molstruc.2020.129543>
24. Ariyanta HA, Ivandini TA, Yulizar Y (2021) A novel way of the synthesis of three-dimensional (3D) MoS₂ cauliflower-like structures using allicin. *Chem Phys Lett*. <https://doi.org/10.1016/j.cplett.2021.138345>
25. Uwazie JN, Yakubu MT, Ashafa AOT, Ajiboye TO (2020) Identification and characterization of anti-diabetic principle in *Senna alata* (Linn.) flower using alloxan-induced diabetic male Wistar rats. *J Ethnopharmacol*. <https://doi.org/10.1016/j.jep.2020.112997>
26. Anitha J, Selvakumar R, Hema S, Murugan K, Premkumar T (2022) Facile green synthesis of nano-sized ZnO using leaf extract of *Morinda tinctoria*: MCF-7 cell cycle arrest, antiproliferation, and apoptosis studies. *J Ind Eng Chem* 105:520–529. <https://doi.org/10.1016/j.jiec.2021.10.008>
27. Vasantharaj S, Sathiyavimal S, Senthilkumar P, Kalpana VN, Rajalakshmi G, Alsehl M, Elfasakhany A, Pugazhendhi A (2021) Enhanced photocatalytic degradation of water pollutants using bio-green synthesis of zinc oxide nanoparticles (ZnO NPs). *J Environ Chem Eng* 9:105772. <https://doi.org/10.1016/j.jece.2021.105772>
28. Astuti S, Yulizar Y, Saefumillah A, Apriandanu DOB (2020) Chitosan nanoparticles modified by polyethylene glycol as lamivudine drug delivery system. *AIP Conf Proc*. <https://doi.org/10.1063/50007925>
29. El Gollit A, Fendrich M, Bazzanella N, Dridi C, Miotello A, Orlandi M (2021) Wastewater remediation with ZnO photocatalysts: green synthesis and solar concentration as an economically and environmentally viable route to application. *J Environ Manage*. <https://doi.org/10.1016/j.jenvman.2021.112226>
30. Yadav S, Rani N, Saini K (2021) Green synthesis of ZnO and CuO NPs using *Ficus benghalensis* leaf extract and their comparative study for electrode materials for high performance supercapacitor application. *Mater Today Proc*. <https://doi.org/10.1016/j.matpr.2021.08.323>
31. Ashar A, Bhatti IA, Siddique T, Ibrahim SM, Mirza S, Bhutta ZA, Shoaib M, Ali M, Taj MB, Iqbal M, Noor S, Mohsin M (2021) Integrated hydrothermal assisted green synthesis of ZnO nano discs and their water purification efficiency together with antimicrobial activity. *J Mater Res Technol* 15:6901–6917. <https://doi.org/10.1016/j.jmrt.2021.11.009>
32. Aldeen TS, Ahmed Mohamed HE, Maaza M (2022) ZnO nanoparticles prepared via a green synthesis approach: physical properties, photocatalytic and antibacterial activity. *J Phys Chem Solids* 160:110313. <https://doi.org/10.1016/j.jpcs.2021.110313>
33. Sabouri S, Akbari A, Hosseini HA, Darroudi M (2018) Facile green synthesis of NiO nanoparticles and investigation of dye degradation and cytotoxicity effects. *J Mol Struct* 1173:931–936. <https://doi.org/10.1016/j.molstruc.2018.07.063>
34. Anaraki Firooz A, Ghalkhani M, Faria Albanese JA, Ghanbari M (2021) High electrochemical detection of dopamine based on Cu doped single phase hexagonally ZnO plates. *Mater Today Commun* 26:101716. <https://doi.org/10.1016/j.mtcomm.2020.101716>
35. Dogan B, Uslu B, Suzen S, Ozkan SA (2005) Electrochemical evaluation of nucleoside analogue lamivudine in pharmaceutical dosage forms and human serum. *Electroanalysis* 17:1886–1894. <https://doi.org/10.1002/elan.200503307>
36. Purohit B, Vernekar PR, Shetti NP, Chandra P (2020) Biosensor nanotechnology: design, operation, and implementation for biomolecular analysis. *Sensors Int* 1:100040. <https://doi.org/10.1016/j.sintl.2020.100040>
37. Carbone M, Nesticò A, Bellucci N, Micheli L, Palleschi G (2017) Enhanced performances of sensors based on screen printed electrodes modified with nanosized NiO particles. *Electrochim Acta* 246:580–587. <https://doi.org/10.1016/j.electacta.2017.06.074>
38. Shayani H (2019) Electrochemical study of adsorption and electrooxidation of 4, 4' - biphenol on the glassy carbon electrode: determination of the orientation of adsorbed molecules. *Monatshefte Für Chem Chem Mon*. <https://doi.org/10.1007/s00706-018-2318-4>
39. Ullah A, Soc JE, Ullah A, Rauf A, Rana A, Qureshi R, Ashiq N, Hussain H, Kraatz H, Badshah A, Shah A (2015) pH dependent electrochemistry of anthracenediones on a glassy carbon electrode. *J Electrochem*. <https://doi.org/10.1149/2.0881503jes>

Publisher's Note

Springer Nature remains neutral with regard to jurisdictional claims in published maps and institutional affiliations.